Mechanochemical energy transduction during the main rotary step in the synthesis cycle of F_1-ATPase

Jacek Czub,[†] Miłosz Wieczór,[†] Bartosz Prokopowicz,[†] and Helmut Grubmüller[*,‡]

[†]*Department of Physical Chemistry, Gdansk University of Technology, ul. Narutowicza 11/12, 80-233 Gdańsk, Poland*

[‡]*Department of Theoretical and Computational Biophysics, Max Planck Institute for Biophysical Chemistry , Am Fassberg 11, 37077 Göttingen, Germany*

E-mail: hgrubmu@gwdg.de

SUPPORTING INFORMATION

Methods

Simulation protocol

All MD simulations were carried out at constant temperature of 300 K and under constant pressure of 1 bar, using Nose-Hoover[1] and Parinello-Rahman[2] methods, respectively. Periodic boundary conditions were imposed in all three directions, and electrostatic interactions were evaluated by the particle mesh Ewald (PME)[3] with a real-space cutoff of 1 nm and a Fourier grid spacing of 0.1 nm. Van der Waals interactions were modeled with the Lennard-Jones potential truncated at 1 nm. Bond lengths were constrained using P-LINCS[4] for the protein and ligands and SETTLE[5] for water. The equations of motion were integrated using the leap-frog algorithm with a 2 fs time step.

Alchemical transformation of ADP into ATP

To provide a starting structure for simulations with the nucleotide binding site of β_{TP} occupied by ATP, a slow-growth simulation was performed on the original ADP-containing system. For this procedure, a dual topology was constructed with dummy atoms representing the phosphate moiety to be grown. The free energy code implemented in Gromacs was used to consecutively switch on van der Waals and Coulombic interactions, gradually moving from state A (ADP) to state B (ATP) over the course of 300 ns, with

standard soft-core potentials employed to avoid singularities. In the topology, all bonded terms remained unchanged except for dihedral angles, which allowed the triphosphate moiety to eventually assume a favorable geometry within the binding site. Importantly, during this transformation, the Arg373 residue of α_{TP} (the so-called arginine finger) moved by ca. 10Åto form a direct hydrogen bonds with the α and β phosphates of ATP (Fig. S...), consistently with the conformation of the ATP-containing binding site found by x-ray crystallography.[6]

Free energy profile for the β conformational transition

As a reaction coordinate describing the main conformational transition of the β subunit in the $\alpha\beta$ heterodimer with bound ATP, we used the projection on the first eigenvector of the covariance matrix computed from 80 x-ray β conformations (i.e., "Conformational coordinate 1" in Fig S1). The free energy profile along this coordinate was determined by umbrella sampling[7] using 30 overlapping windows spaced 0.25 nm apart between -2.5 nm (closed state) to 5 nm (open state). The harmonic potential with a force constant of 100 kJ/(mol·nm^2) was used as the umbrella potential along the chosen coordinate. The initial structures of the $\alpha\beta$ dimer for the windows in the range -2.5–0 nm were extracted from the F_1 complex subject to the enforced-rotation simulation, in which a partial opening of β_{TP} was observed. The dimers were solvated with a 140 mM NaCl aqueous solution in a dodecahedron

box with a minimum distance of 1.5 nm between the protein and the box boundary and simulated according the same MD protocol as that used for the F_1 complex and described in the main text Methods. The initial structures for the range 0–5 nm were produced in additional MD simulation of the solvated $\alpha\beta$ heterodimer in which the β subunit was steered over 300 ns from the initial intermediate conformation (0 nm) to the fully open conformation (5 nm) using a moving harmonic potential with a force constant of 500 kJ/(mol·nm^2. In each of the windows the systems were simulated for 250 ns and the free energy profile was determined from the last 200 ns of simulations using the standard weighted histogram analysis method (WHAM).[8]

Calculation of kinetic parameters

For the calculation of kinetic parameters, the computed free energy profile was modified by including a linear ramp potential due to the F_o motor. In particular, given the free energy input of ∼12 kcal/mol per single 120° rotary step, a linear function with a slope of −0.1 kcal/° was added to the original free energy profile in Fig. 1B to yield the effective potential shown in blue in Fig. S3. The diffusion coefficient for rotation as a function of the rotation angle, shown in red in Fig. S3, was calculated from the umbrella sampling trajectories using a formula by Hummer,[9] and then smoothed and interpolated to produce a continuous profile. Using these input data, the mean first passage time (MFPT) for the transition from the pre-P_i release state

(0°) to the pre-ATP release state (>55°) was calculated for different scaling factors that effectively lowered the free energy barrier. This calculation was performed using two approaches that yielded values in excellent agreement with each other. The first one involved series of 1D Langevin dynamics simulation in the effective potential (24 simulations for each scaling factor) ran using a custom Python script. The resulting averages over 24 first passage times are shown as green dots in the inset of Fig. 1C. The other approach was based upon the analytical formula for MFPT due to Zwanzig,[10] and the corresponding estimate is shown in the inset of Fig. 1C as a solid olive line.

Thermodynamic cost of changes in binding site occupancy

To estimate the energy input required to induce ligand exchange at the nucleotide binding sites following the rotation of the γ-shaft from 0 to 70°, we used a thermodynamic cycle shown in Fig. S2. From single-molecule experiments,[11,12] it is expected that this (main) rotary substep triggers ATP release from the β_{TP} subunit and is accompanied by ADP binding to the β_{E} subunit. Since in our case the β_{E} subunit was initially empty, the corresponding free energy change should also include phosphate binding to β_{E}. From the cycle in Fig. S2, it can be seen that this free energy change, ΔG_{occ}, can be expressed as the difference between the free energies of ATP hydrolysis in the bound and dissociated states:

$$\Delta G_{\rm occ} = \Delta G_u^{\rm ATP} + \Delta G_b^{\rm ADP/P} = \Delta G_b^{\rm hydr} - \Delta G_u^{\rm hydr}.$$

If we approximate $\Delta G_b^{\rm hydr}$ by subtracting the standard binding free energies of the products (ADP and P_i) and the substrate (ATP), and use the expression relating the free energy of hydrolysis in aqueous solution to the actual (physiological) concentrations of the reactants, we obtain

$$\Delta G_{\rm occ} = \Delta G_b^\circ({\rm ADP}) + \Delta G_b^\circ({\rm P}_i) - \Delta G_b^\circ({\rm ATP}) - \Delta G_{\rm hydr}^\circ + \left(RT \ln \frac{[{\rm ADP}][{\rm P}_i]}{[{\rm ATP}]} \right).$$

Finally, by rearranging the above expression, we can express $\Delta G_{\rm occ}$ as follows:

$$\Delta G_{\rm occ} = \Delta G_u({\rm ATP}) + \Delta G_b({\rm P}_i) + \Delta G_b({\rm ADP}) + \Delta G_{\rm syn}^\circ.$$

where the first three components are the free energy changes upon ATP unbinding (from $\beta_{\rm TP}$), P_i binding (to $\beta_{\rm E}$) and ADP binding (to $\beta_{\rm E}$, in the presence of previously bound P_i) at their physiological concentrations, and $\Delta G_{\rm syn}^\circ$ is the standard free energy of ATP synthesis from ADP and P_i (in solution).

From the measured standard binding free energies ($\Delta G_b^\circ({\rm ATP}) = -13.2$ kcal/mol, $\Delta G_b^\circ({\rm P}_i) = -2.73$ kcal/mol and $\Delta G_b^\circ({\rm ADP}) = -9.95$ kcal/mol; the latter obtained in the presence of excess P_i),[13,14] we find the actual free energies of

binding at typical cellular concentrations ([ATP] = 0.001 M, [P_i] = 0.005 M, [ADP]=0.00025 M) to be −9.1, 0.3 and −4.9 kcal/mol, respectively. Using these values and the standard free energy of ATP synthesis of 7.3 kcal/mol ΔG_{occ} is estimated to be 12.0 kcal/mol. The contribution due to phosphate binding is relatively small and the cost of ATP to ADP exchange alone should be similar in magnitude (14.7 kcal/mol, if we assume constant P_i concentration in solution).

It is also worth noting that $\Delta G_b^{\mathrm{hydr}}$ calculated from the standard free energies of binding is close to zero (0.54 kcal/mol) which is consistent with reversible nature of binding-site hydrolysis/synthesis occurring with an equilibrium constant close to 1.[15,16]

Force distribution analysis

The force distribution analysis (FDA) was performed using a modified version of Gromacs 4.5.3 that includes an implementation of the FDA module.[17,18] For the visual analysis of force distribution, residue-wise forces (i.e., forces between pairs of residues, summed over constituent atoms) were calculated and averaged over individual 400 ns long umbrella sampling trajectories. For the purpose of analysis, electrostatic interactions were cut off at 2.0 nm. Distributions of mean inter-residue forces in two initial (2.5° and 7.5°) and two middle (62.5° and 67.5°) umbrella sampling windows were taken as reference distributions in the pre-P_i release state and the pre-ATP release state,

respectively. Accordingly, changes in force distributions were calculated by subtracting the reference distribution from the average distribution at a given rotation angle, with the first reference distribution used for the 30–60° range and second for the 90–120° range. These changes were then either directly visualized as cylinders (with cylinders scaled and color-coded according to the magnitude and sign of the change in force), or mapped onto the structures with color-code denoting the summed absolute values of all changes in residue-wise force experienced by the given residue.

For the principal component analysis (PCA), a similar scheme was employed, but to generate more data points force averaging was performed over shorter 10 ns subtrajectories. Inter-residue forces that were on average smaller than a threshold of 1 kJ/(mol·nm) were not included in further analysis to limit the size of the covariance matrix. No feature scaling was performed on the force distributions, assuring that only sufficiently large and strongly correlated forces would contribute to first eigenvectors. Four eigenvectors, corresponding to the largest eigenvalues of the covariance matrix, were visualized as networks using the FDA library in VMD,[18,19] with cylinders scaled and color-coded according to the magnitude and sign of individual components of the eigenvector, respectively. Each of these representations identifies correlated changes in pairwise interactions between residues, hence corresponding to collective strain propagation networks. From the projections of actual force distributions on the dominant eigenvectors, the first two

were found to capture relevant modes of force transmission: the projection on the first eigenvector increases monotonously over the whole 120° range, correlating with the overall free energy expenditure during the rotary step, while in case of the second, energy accumulation peaks in the pre-ATP-release state at 70° and subsequently falls off. For the purpose of clarity, smallest components of the four depicted eigenvectors (squared normalized value less than 0.0025) were omitted in visualization.

References

(1) Nosé, S. *J Chem Phys* **1984**, *81*, 511.

(2) Parinello, M.; Rahman, A. *J Appl Phys* **1981**, *52*, 7182–7190.

(3) Essmann, U.; Perera, L.; Berkowitz, M. L.; Darden, T.; Lee, H.; Pedersen, L. G. *J Chem Phys* **1995**, *103*, 8577–8593.

(4) Hess, B. *J Chem Theory Comput* **2008**, *4*, 116–122.

(5) Miyamoto, S.; Kollman, P. A. *J Comput Chem* **1992**, *13*, 952–962.

(6) Abrahams, J.; Leslie, A.; Lutter, R.; Walker, J. *Nature* **1994**, *370*, 621–628.

(7) Torrie, G. M.; Valleau, J. P. *J Comput Phys* **1977**, *23*, 187–199.

(8) Kumar, S.; Bouzida, D.; Swendsen, R. H.; Kollman, P. A.; Rosenberg, J. M. *J Comput Chem* **1992**, *13*, 1011–1021.

(9) Hummer, G. *New J Phys* **2005**, *7*, 34.

(10) Zwanzig, R. *Proc Natl Acad Sci U S A* **1988**, *85*, 2029–2030.

(11) Suzuki, T.; Tanaka, K.; Wakabayashi, C.; Saita, E.-i.; Yoshida, M. *Nat Chem Biol* **2014**, *10*, 930–936.

(12) Watanabe, R.; Iino, R.; Noji, H. *Nat Chem Biol* **2010**, *6*, 814–820.

(13) Weber, J.; Wilke-Mounts, S.; Lee, R.; Grell, E.; Senior, A. *J Biol Chem* **1993**, *268*, 20126–20133.

(14) Senior, A. E.; Nadanaciva, S.; Weber, J. *Biochim Biophys Acte – Bioenergetics* **2002**, *1553*, 188–211.

(15) Boyer, P. *Annu Rev Biochem* **1997**, *66*, 717–749.

(16) Liu, M. S.; Todd, B.; Sadus, R. J. *Biochim Biophys Acta – Proteins and Proteomics* **2004**, *1698*, 197–202.

(17) Xiao, S.; Stacklies, W.; Cetinkaya, M.; Markert, B.; Graeter, F. *Biophys J* **2009**, *96*, 3997 – 4005.

(18) Stacklies, W.; Seifert, C.; Graeter, F. *BMC Bioinform* **2011**, *12*, 1–5.

(19) Humphrey, W.; Dalke, A.; Schulten, K. *J Mol Graph* **1996**, *14*, 33–38.

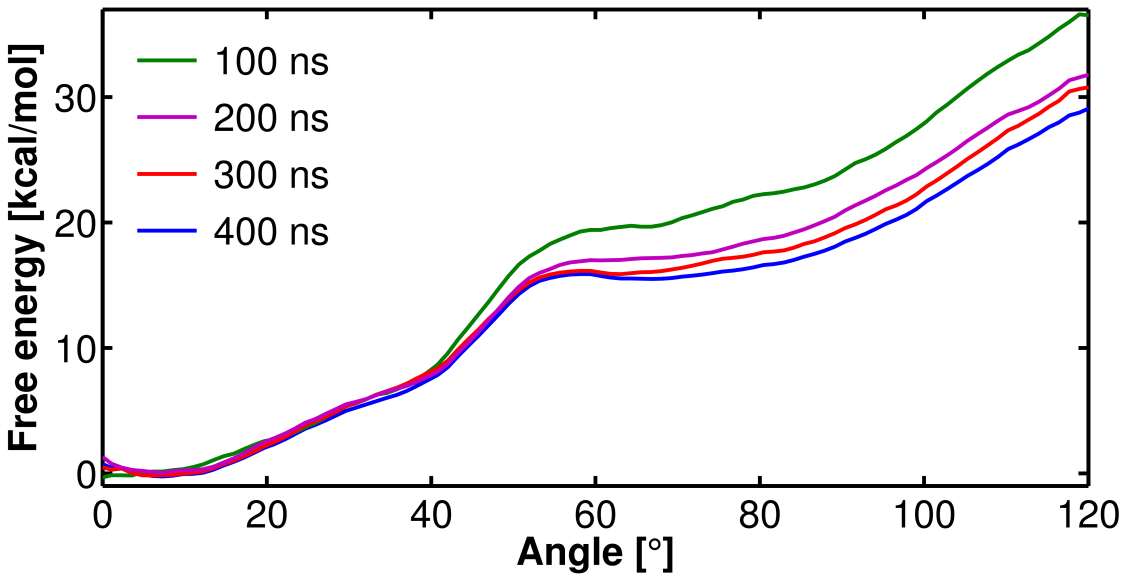

Fig. S1: Convergence of the free energy profile with the length of umbrella sampling trajectories taken for analysis. Most pronounced changes of the slope in the 60–80° interval suggest that in this region the free energy is less converged, with the second shallow minimum showing a tendency to get deeper with increasing sampling.

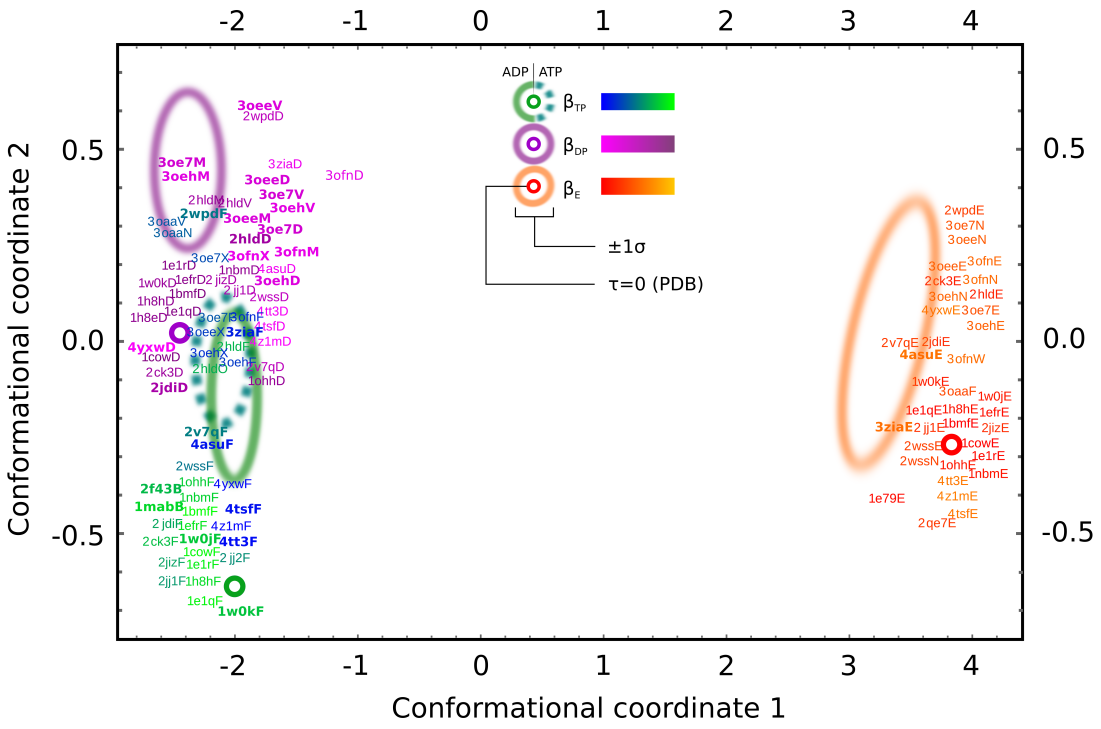

Fig. S2: Distribution of 80 crystal structure conformations of the β subunit (with resolution >3.5 Å) on the plane of greatest structural variability spanned by two first eigenvectors of the positional covariance matrix computed for a common subset of C_α atoms. β_{TP} subunits are colored green to blue, β_{DP} subunits magenta to purple, and β_E subunits orange to red. The green, purple and red dots mark the location of the initial structure in our equilibrium simulations (1E79), and the semi-transparent ellipses denote the regions of the conformational space explored by individual β subunits in these simulations ($\pm\sigma$). For β_{TP}, data are shown for either ATP or ADP present in the active site. Bold font is used to indicate subunits in which nucleotide occupancy differs from the default case (i.e., empty β_{TP} or β_{DP} subunit or nucleotide-bound β_E subunit) to show that the active site occupancy alone has little effect on the conformational state of the subunit in F_1 complex . In cases where dense packing of the labels caused them to overlap, they were repositioned slightly to increase readability.

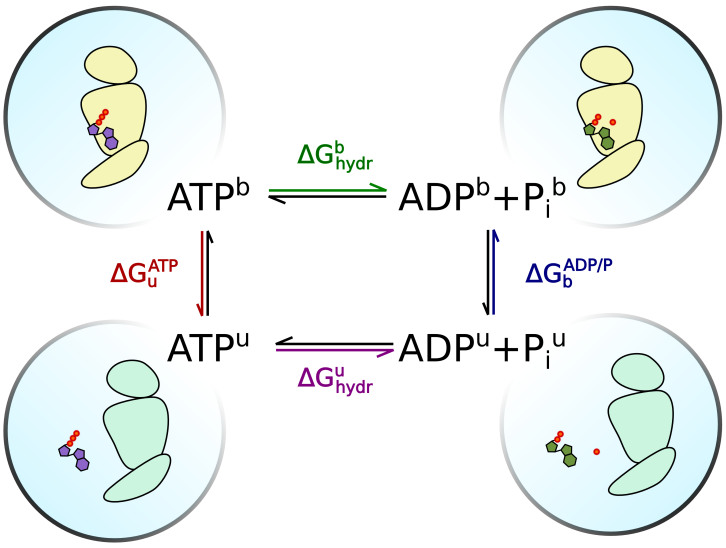

Fig. S3: Thermodynamic cycle used for estimating the free energetic cost of the change in binding site occupancy following the main rotary substep in the synthetic cycle (see SI Methods for details).

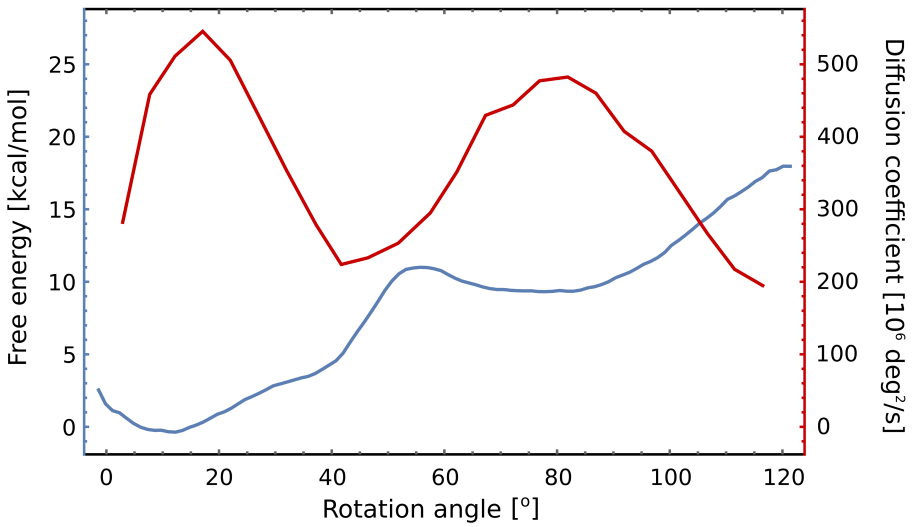

Fig. S4: The free energy profile modified by adding F_o-generated torque potential with a constant slope (blue; see main text) and the diffusion coefficient in the angular coordinate (red) as a function of the γ-shaft rotation angle, used in the estimation of barrier-crossing rates. The diffusion coefficient was calculated in each umbrella sampling window as the quotient of the variance in the angular coordinate and the autocorrelation time (see SI Methods).

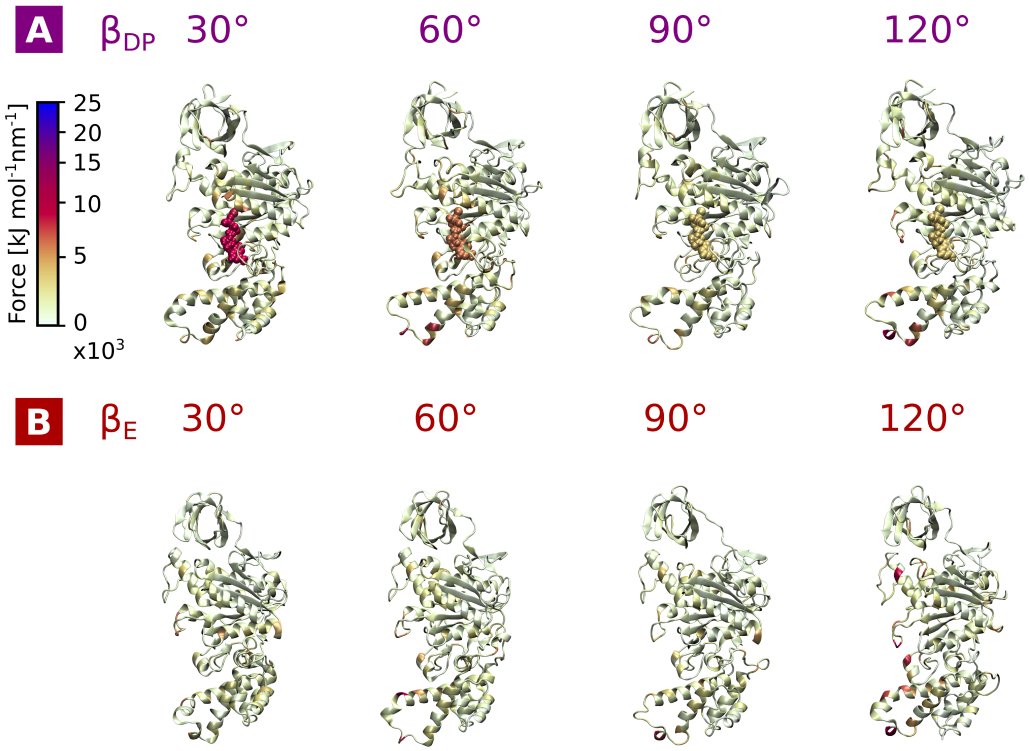

Fig. S5: Changes in inter-residue forces observed at respective γ-shaft rotation angles for the two other β subunits (β_{DP} and β_E; see Fig. 4A for comparison). Note that during most of the rotation cycle, the β_{DP}-bound nucleotide remains almost intact, in contrast to the β_{TP}-bound one.

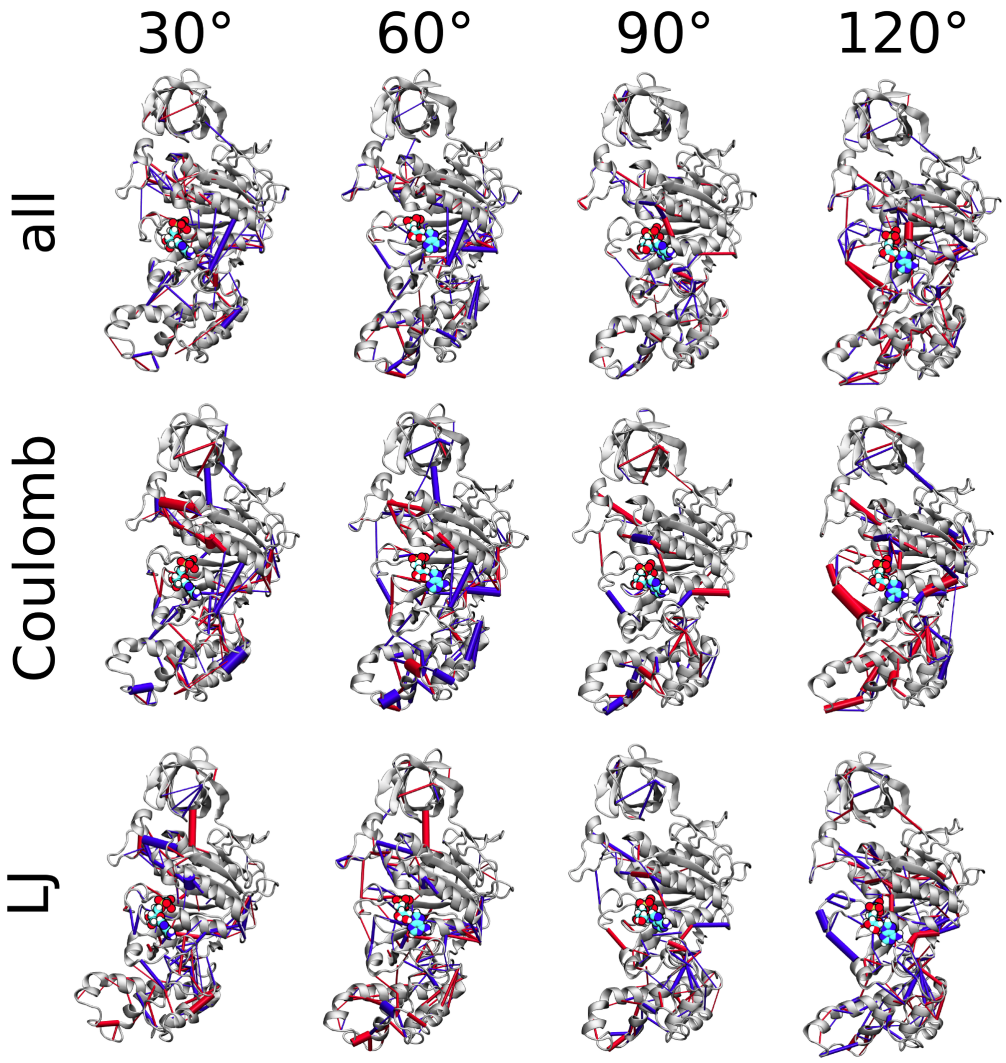

Fig. S6: Changes in inter-residue forces observed at respective γ-shaft rotation angles decomposed into contributions from electrostatic (Coulombic) and steric (Lennard-Jones, LJ) interactions. Scale is preserved across all panels so that cylinder radii are proportional to the magnitude of observed changes in force. Only forces within the β subunit were taken into account.

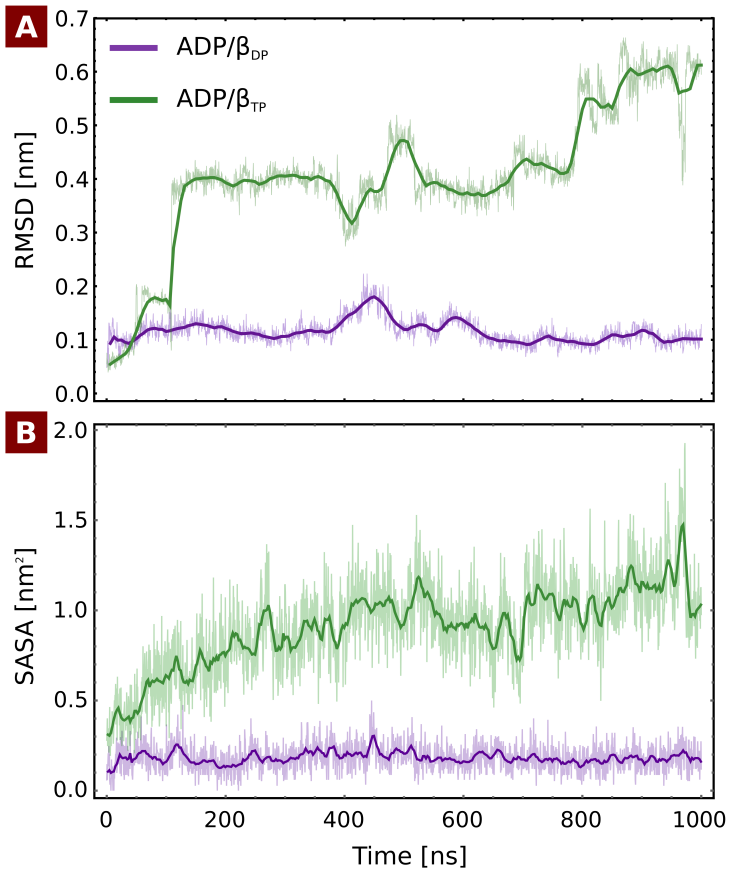

Fig. S7: Root-mean square deviation (RMSD) and solvent-accessible surface area (SASA) of the active site-bound nucleotides in β_{DP} and β_{TP} during the course of a 120° rotation of the γ-shaft. In the active site of β_{TP}, the nucleotide is seen to be bound less tightly and becomes gradually exposed to the solvent in the α/β cleft.

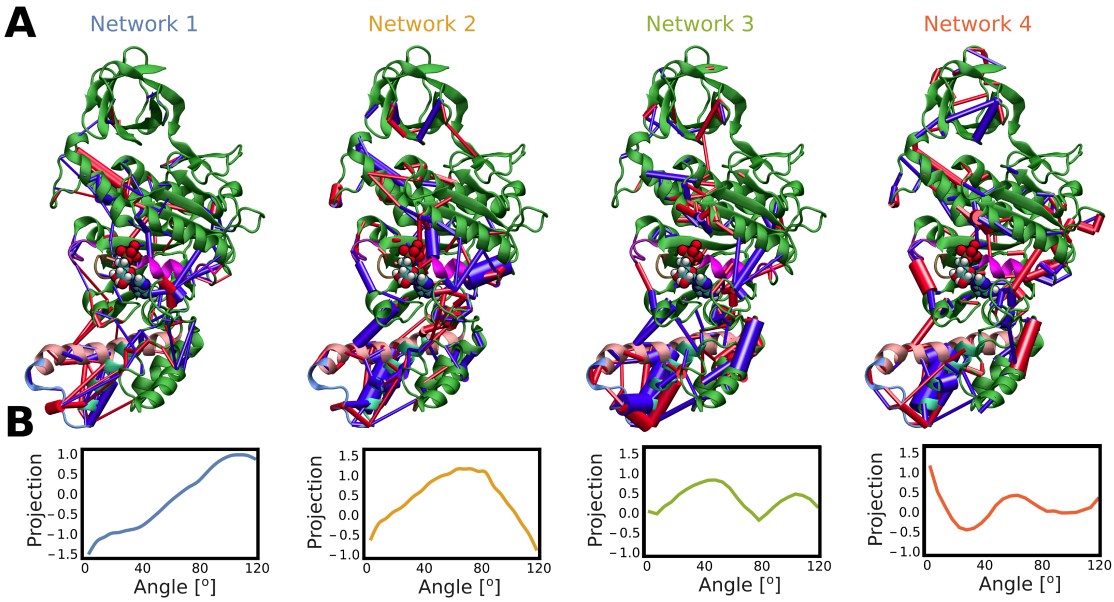

Fig. S8: Main allosteric networks involved in force transmission within the β_{TP} subunit calculated as the first four force PCA eigenvectors (see Fig. 5 and SI Methods for details). In the case of networks 1 and 2, the energy stored coincide with the features of the free energy profile, namely the overall increase (1) and a shallow minimum at ca. 70° (2). Contrary to the first two, projections on eigenvectors 3 and 4 do not correlate with the free energy profile and hence cannot be interpreted in a straightforward manner.

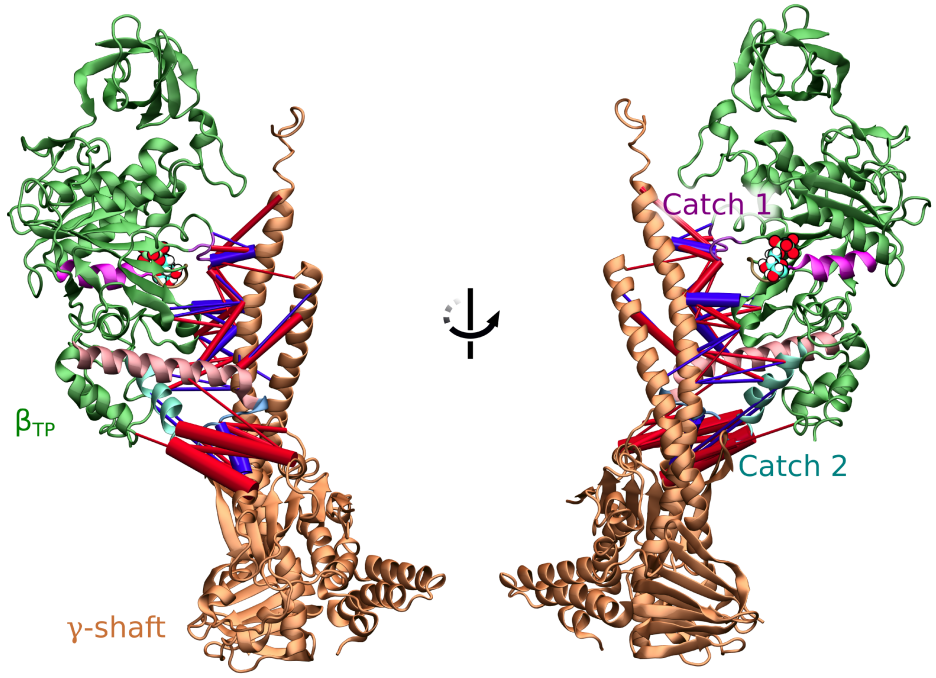

Fig. S9: Direct force transmission between the γ-shaft and β_{TP}, shown at the rotation angle of 60°. Note that both the catch 1 and catch 2 loops (see Fig. 1A), as well as the short helix situated between them at the β/γ interface, can all be involved in force transduction.

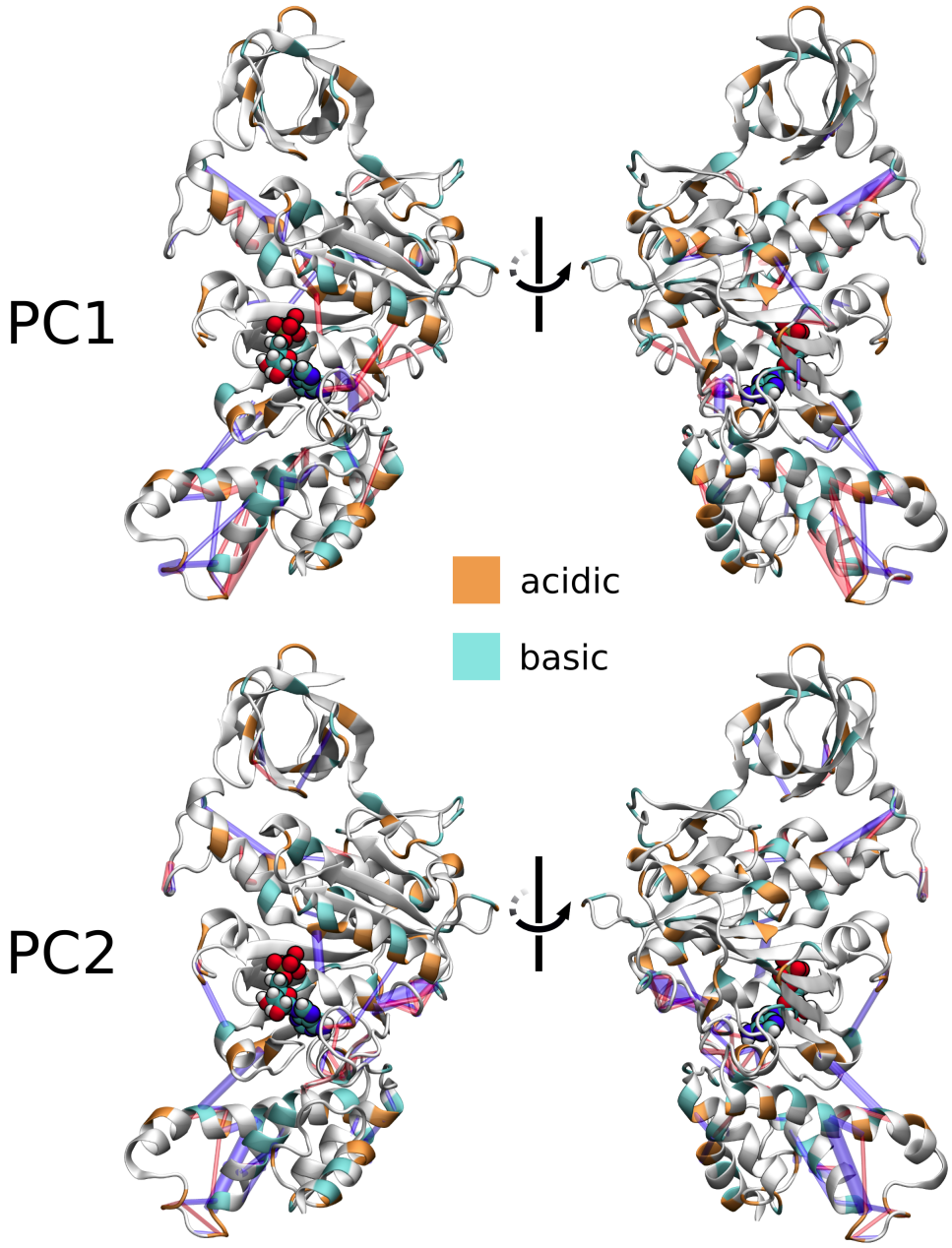

Fig. S10: Distribution of charged (acidic and basic) amino acids superimposed on the two major allosteric networks (see Fig. 5 for comparison). Note that majority of contributions correspond to charged pairs (salt bridges).

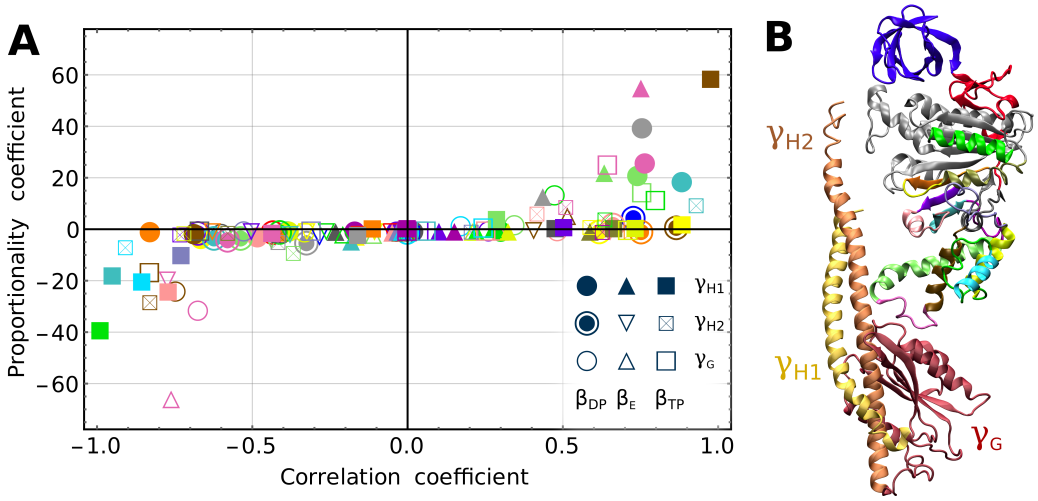

Fig. S11: Correlations between the energy of interaction between structural features of the β and γ subunits and the free energy profile for the rotation of the γ-shaft in the 70–120° range. Based on structural features, the γ subunit was divided into 3 and each of the three β subunits into 19 parts (see coloring in panel B), and interaction energies for all possible 171 $\gamma\beta$ pairs were calculated as a function of rotation angle by Boltzmann-reweighting the umbrella sampling ensemble. For every such profile, we calculated proportionality coefficients (as a measure of the magnitude of the energetic contribution) and linear correlation coefficients with the free energy profile. The interaction between helix 2 of β_{TP} and helix 1 of γ, marked as A solid brown square, shows highest correlation with the free energy profile and, at the same time, is largest in magnitude, which prompted us to create a variant of the protein with all charged residues in helix 2 of β_{TP} mutated to alanines (see Fig S9).

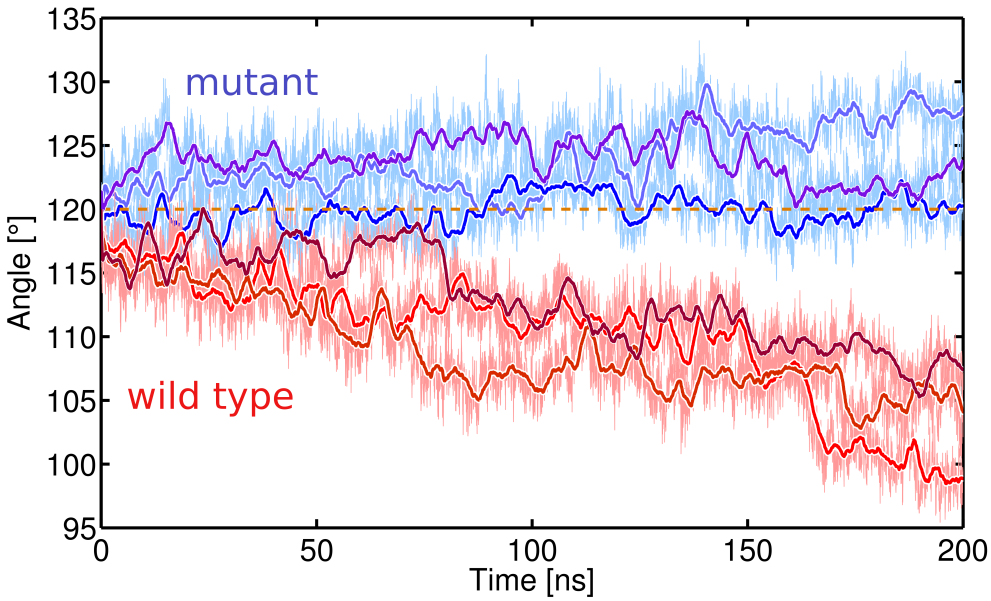

Fig. S12: Spontaneous rotation of the γ-shaft in equilibrium simulations initialized from the 120° state. The wild-type protein rotates back to return towards the pre-ATP-release state, while the mutations (K401A, R406A, R408A and K406A) appear to abolish this tendency. Three independent 200 ns simulations were performed for the mutant and wild type forms.

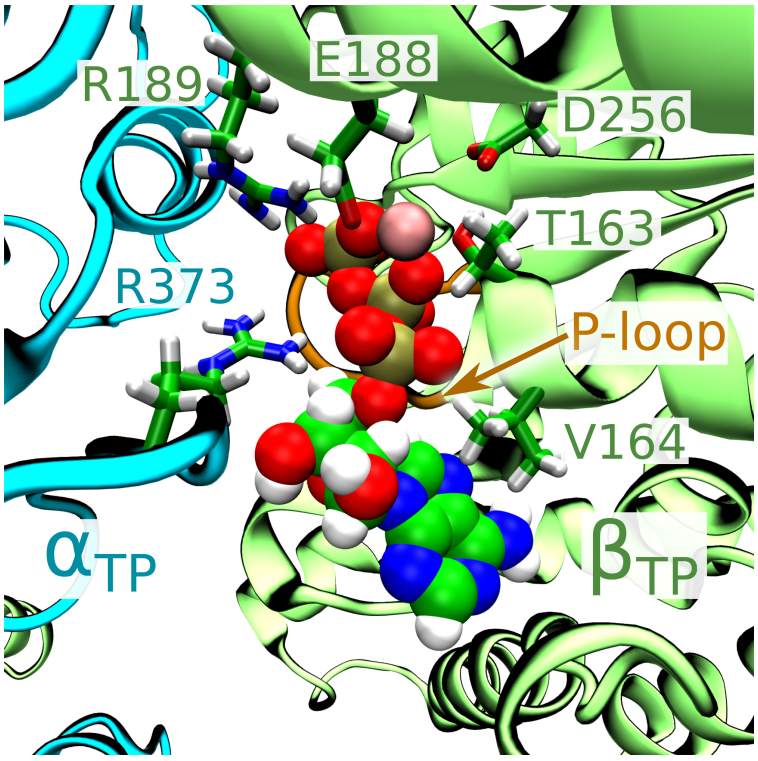

Fig. S13: Structure of the β_{TP} binding site after alchemical transformation of ADP into ATP. Note that the so-called arginine finger (α_{TP}R373) is in direct contact with the phosphate moiety of the nucleotide molecule.

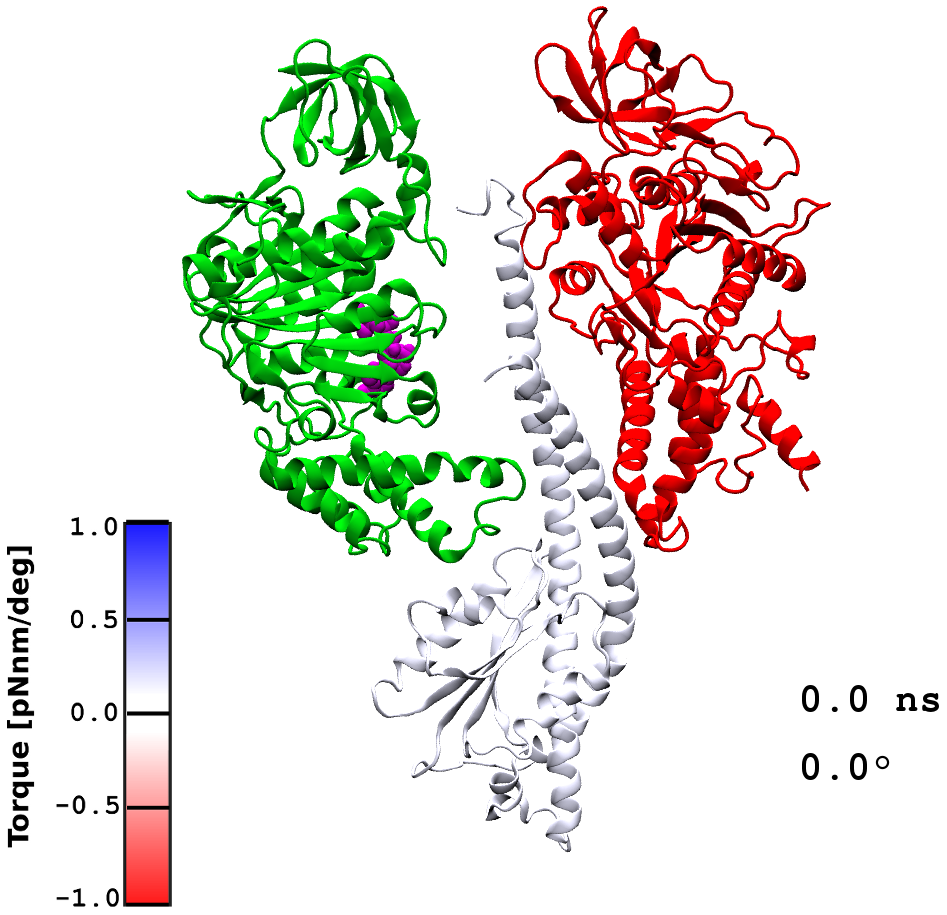

Movie S1: Enforced flexible-axis rotation of the γ-shaft used to produce the initial geometries for free energy simulations (sideview). The torque due to external potential is color-mapped onto the γ subunit. β_{TP} is shown in green and β_E in red.

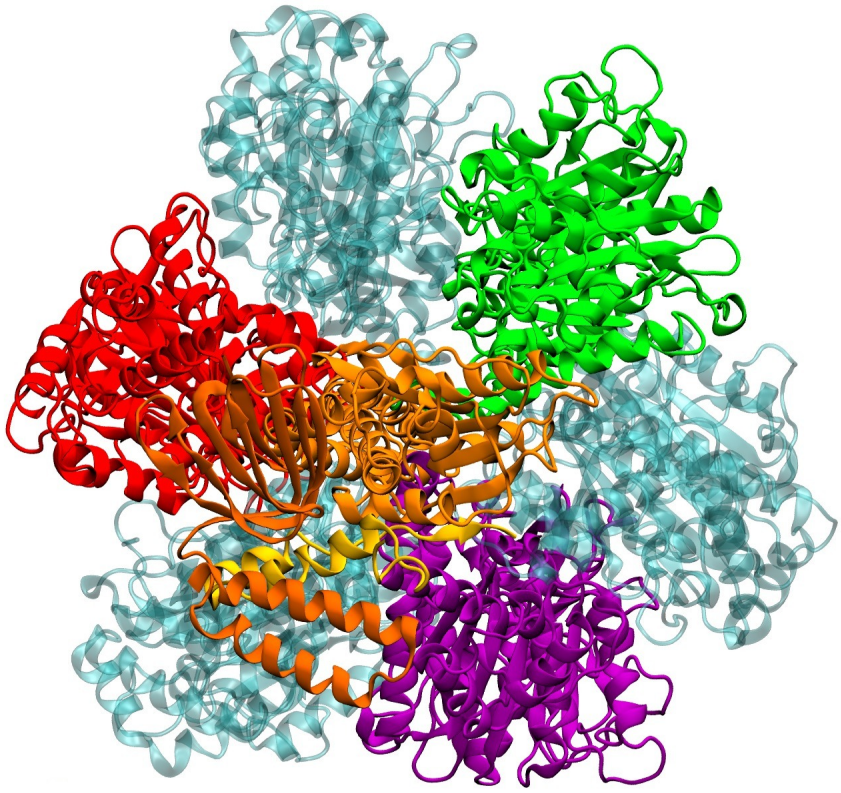

Movie S2: Enforced flexible-axis rotation of the γ-shaft used to produce the initial geometries for free energy simulations (bottom view).

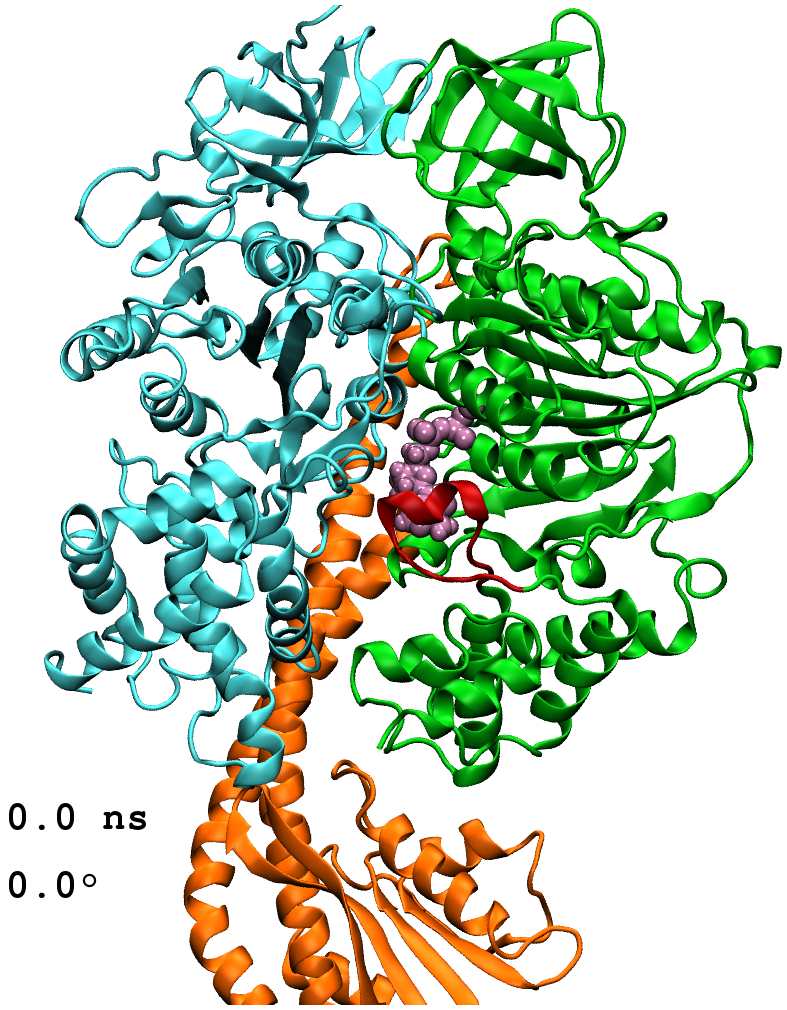

Movie S3: Gradual displacement of the lid-like loop (shown in red) associated with increased conformational freedom of the β_{TP}-bound nucleotide (pink) during the enforced rotation simulation.